Advanced Composite Materials
Publication details, including instructions for authors and subscription information:
http://www.tandfonline.com/loi/tacm20

Ellipticity ratio effects in the energy absorption of laterally crushed composite tubes

E. Mahdi , O. M. S. Alkoles , A. M. S. Hamouda & B. B. Sahari

Version of record first published: 02 Apr 2012.

To cite this article: E. Mahdi , O. M. S. Alkoles , A. M. S. Hamouda & B. B. Sahari (2006): Ellipticity ratio effects in the energy absorption of laterally crushed composite tubes, Advanced Composite Materials, 15:1, 95-113

To link to this article: http://dx.doi.org/10.1163/156855106776829374

Adv. Composite Mater., Vol. 15, No. 1, pp. 95–113 (2006)

Also available online - www.vsppub.com

Ellipticity ratio effects in the energy absorption of laterally crushed composite tubes

E. MAHDI [1,*], O. M. S. ALKOLES [1], A. M. S. HAMOUDA [2] and B. B. SAHARI [2]

[1] *Aerospace Engineering Department, University Putra Malaysia, 43400 UPM, Serdang, Selangor, Malaysia*

[2] *Mechanical and Manufacturing Engineering Department, Faculty of Engineering, University Putra Malaysia, 43400 UPM, Serdang, Selangor, Malaysia*

Received 7 November 2004; accepted 11 July 2005

Abstract—A comprehensive experimental investigation of woven roving glass/epoxy laminated composite elliptical tubes subjected to quasi-static lateral loading has been carried out. To this end a series of experiments were conducted for tubes with ellipticity ratio a/b ranging from 0.5 to 2. Typical deformation histories of the tubes are presented and influences thereon of ellipticity ratio are discussed. It was found that for $a/b > 1$, two fracture lines developed, whereas for $a/b < 1$ only one fracture line was observed to develop. Modes of energy dissipation mechanisms are identified and analysed on the basis of micro and macro failure levels. Ellipticity ratio significantly affected the energy absorption capability of the tubes.

Keywords: Tubes; ellipticity ratio; energy dissipation; crush loads; lateral collapse.

NOMENCLATURE

A	cross-sectional area of material
A_2	cross-sectional area occupied by the structure
a, a_o	major axes, in which the load is applied
b, b_o	minor axes
a/b	ellipticity ratio
CFE	crush force efficiency $= P_m/P_{HP}$
CS	crushed strain $= u/2a$
E_{NS}	normalised energy absorbed

Edited by the JSCM.

*To whom correspondence should be addressed. E-mail: elsadig@eng.upm.edu.my

E_S	crushing energy absorbed per unit mass
E_V	crushing energy absorbed per unit volume
P_i	instantaneous crush failure load
P_m	average crush failure load
P_{HP}	highest peak crush failure load
Set 1	tubes with ($a/b = 0.5, 0.57, 0.67$)
Set 2	tubes with ($a/b = 0.8, 1, 1.25$)
Set 3	tubes with ($a/b = 1.5, 1.75, 2$)
t	thickness of the tube wall
u	crushed distance
V	initial space volume occupied by the structure
W	width of the tube wall

Greek

σ_m	average crush stress

1. INTRODUCTION

Crushing behaviour of composite elliptical tubes subjected to axial compression has been investigated both experimentally and numerically by the authors [1]. A number of different failure modes were observed. It is noted that the ellipticity ratio significantly influenced the energy absorption capabilities. However, any energy absorbing system must be insensitive to the loading directions, especially lateral loading during the side impact event.

Laterally loaded cylindrical cluster have been effectively employed as energy dissipaters in impact attenuation devices. They exhibit a favourable load-deformation characteristic. An important class of impact attenuation device are crash cushions used in a car as bumpers for safety purposes. They are designed to stop vehicles during impact events avoiding serious injuries to occupants [2, 3]. Therefore, the lateral collapse of metallic and composite tubes with circular cross-section has earlier been examined extensively through experiments and mathematical modelling [4–9]. Studies of lateral collapse behaviour of metallic and composite tubes with elliptical cross-section are however still scarce.

Wu and Carney [10, 11] investigated the collapse behaviour of braced metallic elliptical tubes under lateral compressive load. They introduced their investigated structure to the field of crashworthiness as impact attenuation devices in roadside safety application. To date there are no experimental data available in the literature on the energy absorption capabilities of composite elliptical tubes under lateral compressive load.

This paper considers the behaviour of composite elliptical tubes subjected to quasi-static lateral loading wherein the load is applied at the top and bottom sides of

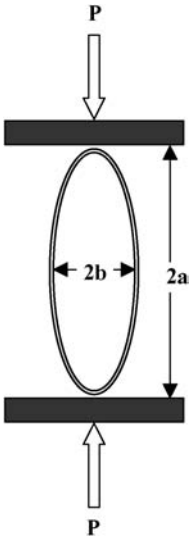

Figure 1. Notation of lateral test of elliptical tube.

the tube through flat platens as shown in Fig. 1. The wet wrapping process was used to fabricate the specimens. More details about the fabrication process are also given in Ref. [1]. Four layers of woven roving glass fibre/epoxy were wrapped to get the thickness of about 3.5 mm. All the specimens were compressed up to material densification stage at cross-head speed of 15 mm/min. Since the energy absorbed is very much dependent on the specific failure mechanism, which can vary from test to test even when all parameters are kept constant, the results are presented from the average of three tests and the repeatability of the results was found to be very good. Failure mode was investigated using the photographs taken while crushing the specimens. The photographs at any experiment were taken during the test; thus the photograph shows the specimen at some different stress level.

2. DEFORMATION MODES

Figures 2 to 12 illustrate the key results obtained from the quasi-static crushing tests. The experimental data from the measured load–displacement responses are summarised in Table 1. The tubes are divided into three sets based on their mode of failure and the appearance of load–displacement curves.

2.1. Set 1 ($a/b = 0.5, 0.57, 0.67$)

Figures 2a and 2b show the representative deformation process and the corresponding load-deflection curve for a tube with a/b ratio $= 0.67$. Since both the top and bottom portions of these types of tubes have small curvatures, the tubes have experienced much deformation during the initial collapse stage. This in turn leads

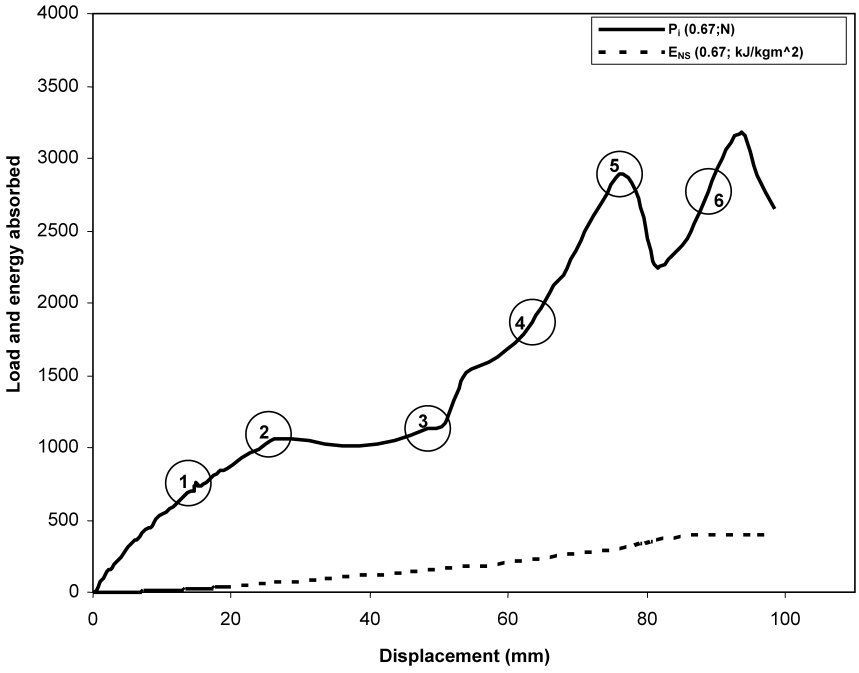

(a)

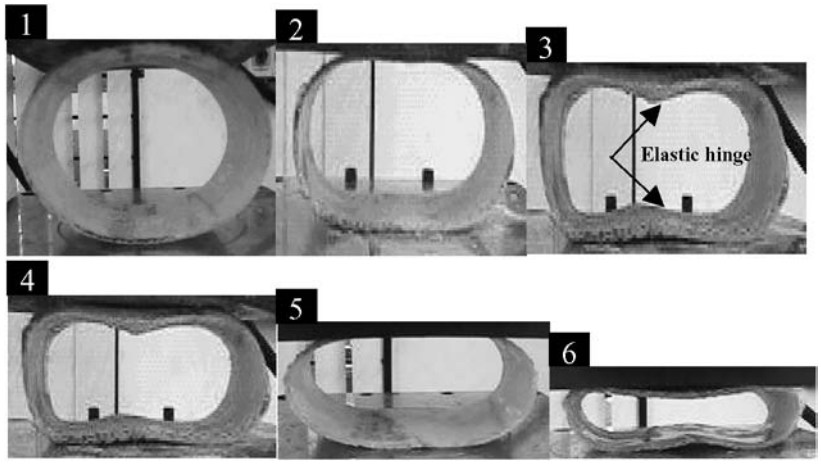

(b)

Figure 2. (a) Load–displacement and absorbed energy curves for tube with $a/b = 0.67$; (b) deformation history for tube with $a/b = 0.67$.

to crazing and cracking of the polymer matrix and a rapid increase in the friction coefficient between the bottom end of the tube and the platen; hence, the bottom elastic hinge forms and undergoes significant rotation which results in a drop in load-carrying capacity. When the bottom hinge touches the upper part of the tube,

Table 1.
Crashworthiness parameters for composite elliptical tubes

a/b	a (mm)	P_m (N)	P_{HP} (N)	CFE (N/N)	CS (mm/mm)	E_{NS} kJ/(kgm^2)	E_V (kJ/m^3)	σ_m (MPa)
Set 1								
0.50	79.70	1145	1768	0.65	0.83	527.35	129.25	0.86
0.57	90.86	1011	1545	0.65	0.89	442.05	104.60	0.73
0.67	106.80	812	1060	0.77	0.91	344.09	78.85	0.55
Set 2								
0.80	127.52	778	922	0.84	0.89	275.57	61.56	0.49
1.00	159.40	729	873	0.84	0.94	225.00	50.00	0.42
1.25	159.40	673	912	0.74	0.94	337.00	75.00	0.42
Set 3								
1.50	159.40	951	1074	0.89	0.94	396.00	91.00	0.65
1.75	159.40	1296	1791	0.72	0.94	464.00	110.00	0.93
2.00	159.40	1477	1561	0.95	0.94	520.00	127.00	1.11

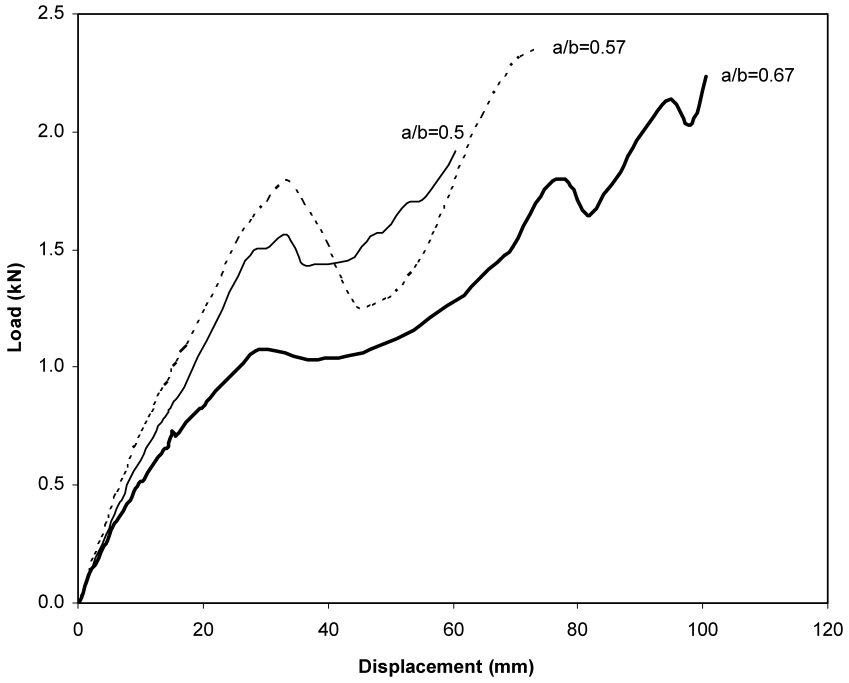

Figure 3. Load–displacement curves for Set 1.

the rotation is restrained by the upper part and the tube resistance is recovered. It is seen that as a/b ratio increases, large fluctuations of load occur. Tubes with a/b ratio equal to 0.5 displayed the smoothest characteristics of load–deformation curve as shown in Fig. 3.

2.2. Set 2 ($a/b = 0.8, 1, 1.25$)

Typical load–deformation and energy compression curves of composite tube with a/b ratio $= 0.8$ are shown in Figs 4a and 4b. The load–deformation curves are characterized by fewer peaks. Unlike other tubes and, in this set, elliptical tube does not show sudden or gradual drop in load. All the tubes of this set experienced flattening deformation in the pre-collapse stage. It is also evident that more deformation occurs at the bottom half of the tube. This is attributed to the fact that the upper half is subjected to smaller forces less by an amount equal to the magnitude of the friction forces than the bottom half of the tube and hence undergoes lesser, but similar, deformations. The occurrence of an elastic hinge at the bottom surface of the tube tends to weaken the tube. It is observed that collapse initiation is influenced by ellipticity ratio and, as a/b ratio increases, the initial collapse deformation increases as shown in Fig. 5. Weakening in tube resistance is being balanced by the formation of resultant forces at the left and right hand sides of the tube wall. Consequently stable load–deformation curves were observed during the post-collapse stage.

2.3. Set 3 ($a/b = 1.5, 1.75, 2$)

The appearance of the load–deformation curve for this set is similar to the axially loaded composite tubes, where the energy absorbed during the initial collapse stage is small compared to the post-collapse stage (Figs 6, 7). It is observed that the top and bottom halves of the tubes deformed identically as mirror images of each other. In the initial stages of compression, the top and bottom surfaces of the tube in contact with the platens were seen to bend like an inward dimple and fracture lines were seen along the axial direction at the innermost surface of the tube wall. It is evident that the tubes exhibit an unstable behaviour after reaching the first peak load. The initial collapse response of the tubes depends upon their ellipticity ratio and generally the load carrying capacity of the tubes increases as ellipticity ratio increases (see Fig. 8). The load–displacement curves start to recover when the inner surface of bottom and top hinges came into contact. The basic energy dissipation mechanism during the initial collapse stage is bending about the shell generators, producing a flat surface at the top and bottom of the tube and the elastic hinges located at 90° from each other. It is also evident that the formation of fracture lines is the main energy dissipation mechanism during the post-collapse stage. The location of fracture lines was observed to be insensitive to the tube ellipticity ratio. This type of mode is associated to Set 3 (see Figs 6a, 6b). This type of failure was also observed by Burton and Craig [12] in which the central generators under the platens move away from the platens as the deformation progresses. However, the gradual drop-off in load carrying capacity for this set is larger than in other sets.

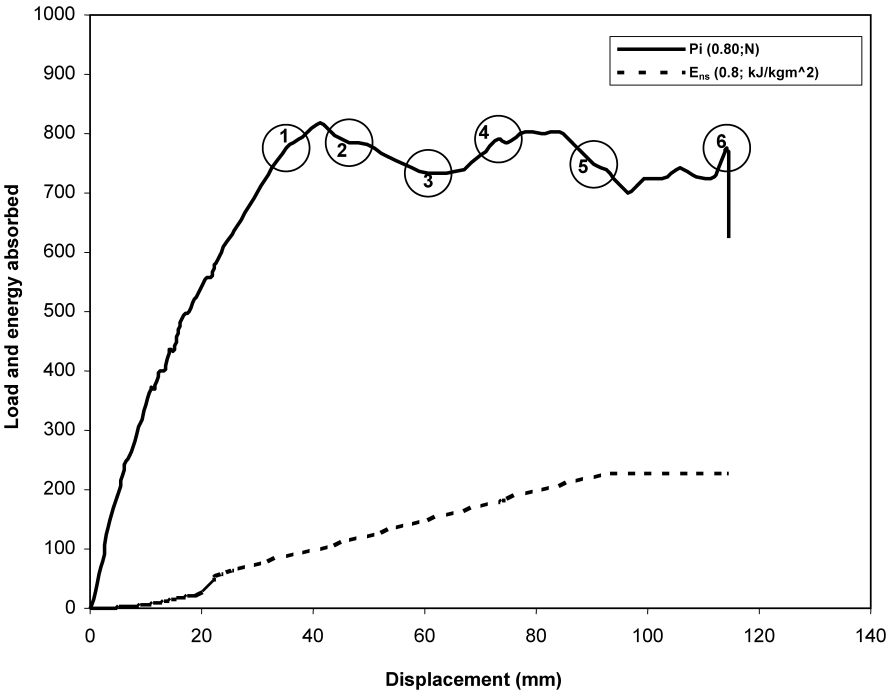

(a)

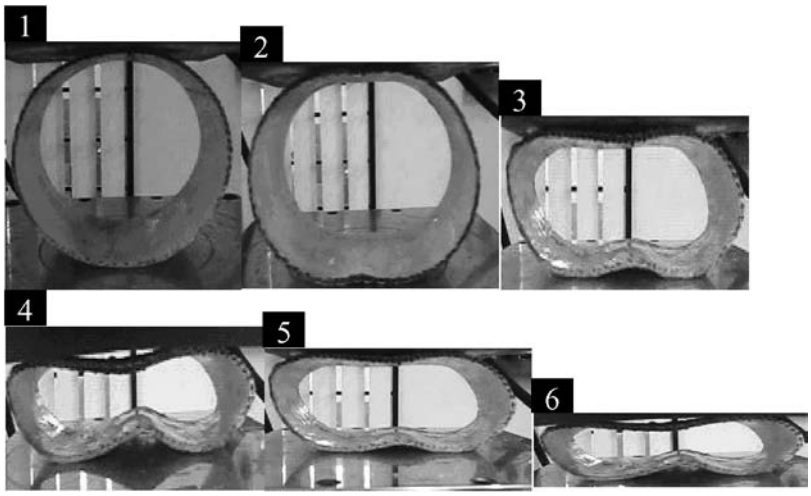

(b)

Figure 4. (a) Load–displacement and absorbed energy curves for tube with $a/b = 0.8$; (b) deformation history for tube with $a/b = 0.8$.

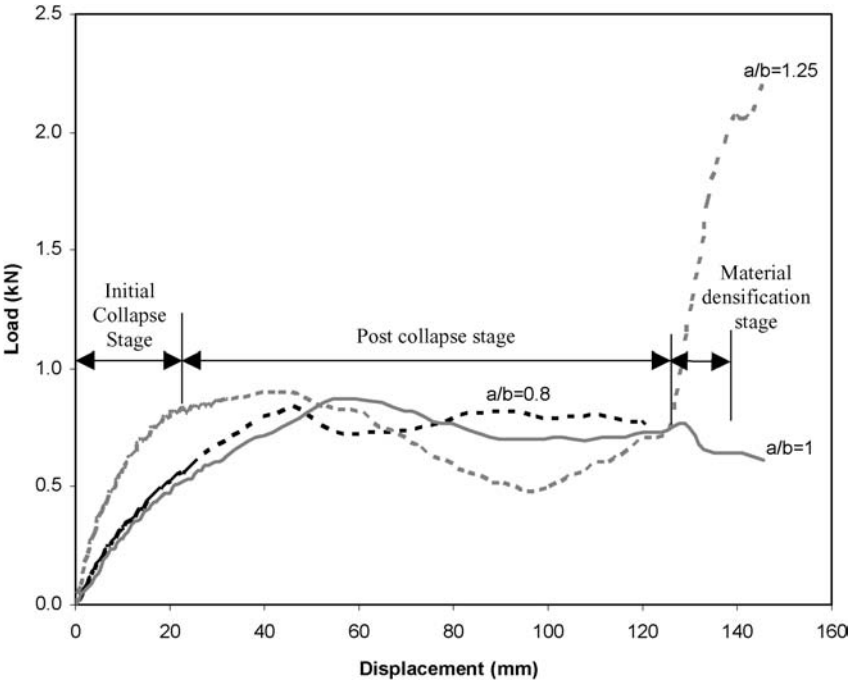

Figure 5. Load–displacement curves for Set 2.

3. CRASHWORTHINESS PARAMETERS

Crashworthiness ensures the vehicle structural integrity and its ability to absorb crash energy with minimal attenuation of survivable space. When evaluating the crashworthiness of energy absorbing devices, attention should be directed to the crush force efficiency (*CFE*), the crushed strain (*CS*) and energy absorption capabilities. This is because, if the initial collapse load is too high, unacceptably high occupant impact decelerations with the collapse of the vehicle interior could result. On the other hand, if the collapse load of the device is too low, the required energy dissipation capacity may not be achieved and the device might bottom out, resulting in dangerously high occupant ridedown decelerations.

3.1. Crush force efficiency (CFE)

The *CFE* is defined as

$$CFE = \frac{P_{\mathrm{m}}}{P_{\mathrm{HP}}}, \tag{1}$$

where P_{HP} and P_{m} represent highest peak and mean crush failure load respectively, in which the mean crush failure load obtained by averaging the crush load values over the crush displacements.

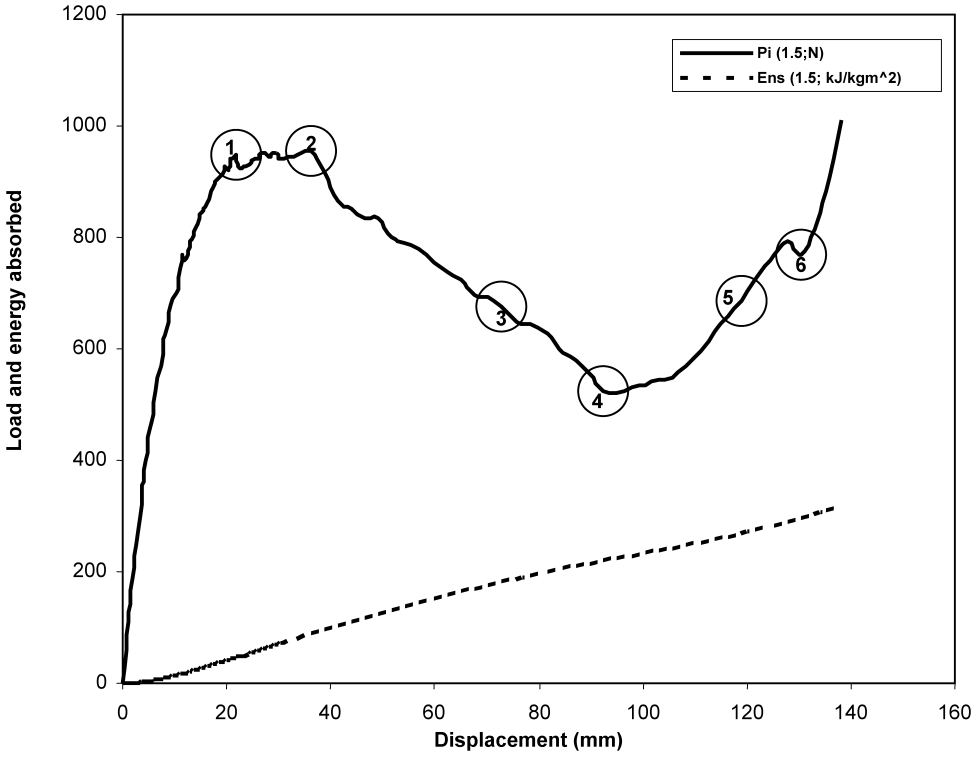

(a)

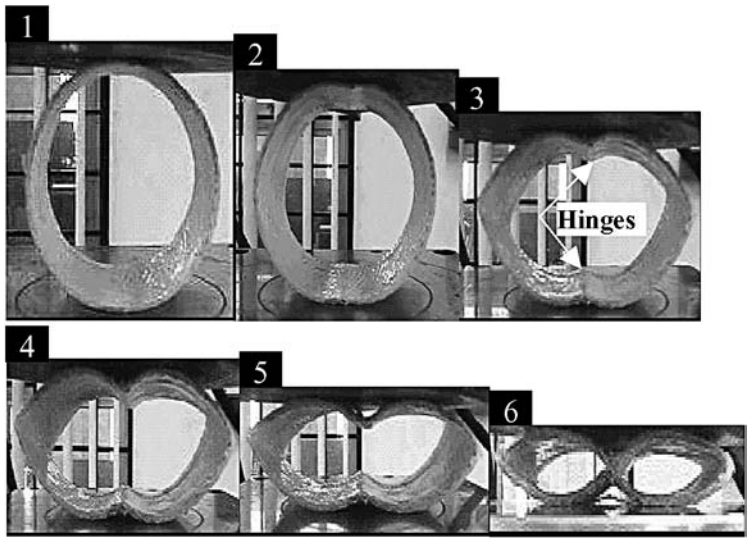

(b)

Figure 6. (a) Load–displacement and absorbed energy curves for tube with $a/b = 1.5$; (b) deformation history for tube with $a/b = 1.5$.

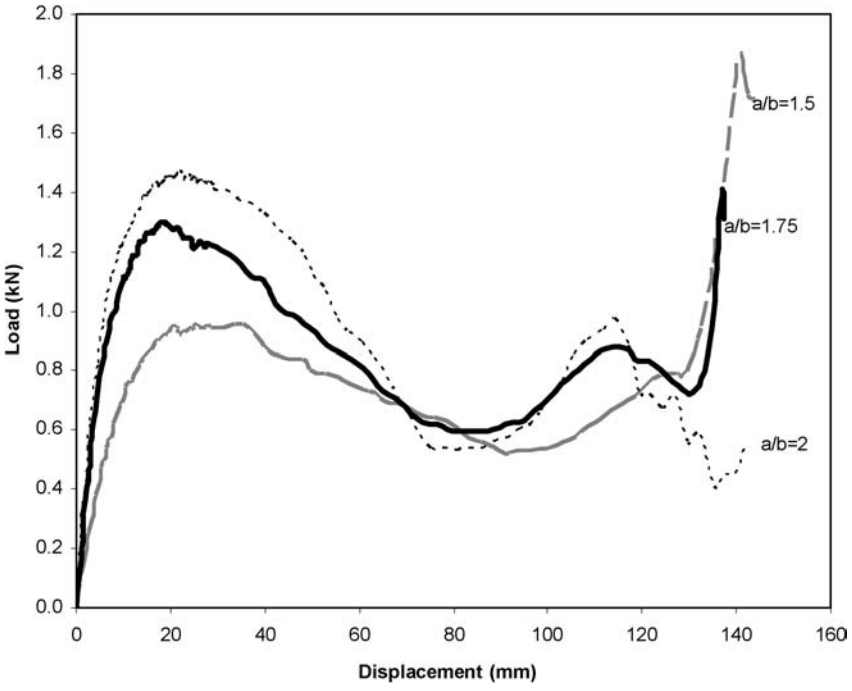

Figure 7. Load–displacement curves for Set 3.

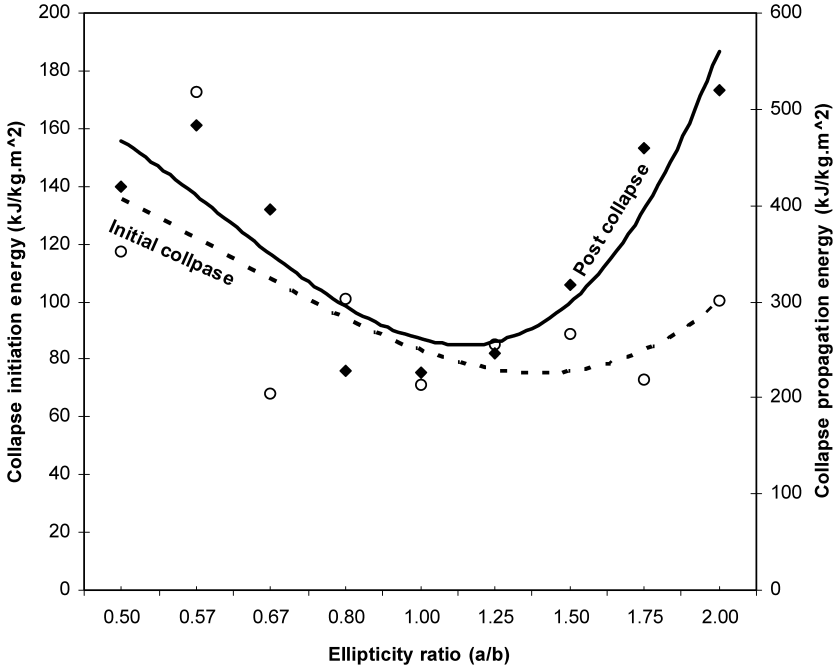

Figure 8. Crashworthiness parameters of laterally crushed composite elliptical tubes.

3.2. Crushed strain (CS)

The desire energy absorber device has crushable structures, which can be defined as crushed strain (*CS*). The *CS* can be obtained by

$$CS = \frac{u}{2a_0}, \tag{2}$$

where u represents the crush distance up to the initiation of material densification phase $2a_0$ represents total height of the structure (major axis).

3.3. Energy absorption capability

Energy absorption capability during the structural crash is an essential requirement for the complete spectrum of passenger transport vehicles. Instantaneous energy absorption capability of the elliptical composite tube was computed by integrating the load–displacement curve as

$$W_{\mathrm{T}} = \int_{s_p}^{s} P_i \, \mathrm{d}s. \tag{3}$$

It is interesting to note that the energy absorption capability can be categorised into two types: these are the specific energy absorption and the volumetric energy absorption. Therefore, the energy absorbed per unit mass, E_{S} is depicted as $E_{\mathrm{S}} = W_{\mathrm{T}}/m$. It should be noted that the above equation is used to compare the specific energy absorption capability of structure with different mass density and same cross-sectional area, while in this study the structure being investigated is with different mass density as well as cross-sectional area. Therefore, the specific energy absorption should be normalised to eliminate the effect of cross-sectional area. This normalisation can only be achieved by dividing the specific energy absorption by the cross-sectional area of the structure as $E_{\mathrm{NS}} = W_{\mathrm{T}}/mA$.

The volumetric energy absorption capability (i.e. energy absorbed per unit volume) is also an essential parameter for energy absorbing system design, where the space is a restraint factor. The volume occupied by a composite elliptical tube before crushing can be calculated as $V = WA_2$, where A_2 is the cross-sectional area occupied by the structure, given by $A_2 = \pi(a+t)(b+t)$. The energy absorbed per unit volume E_{V} can be calculated as $E_{\mathrm{V}} = W_{\mathrm{T}}/V$.

It is seen that elliptical tubes seem to have an advantage over their circular counterparts in that they possess larger collapse strokes and increased normalised specific energy dissipation. Most of Sets 2 and 3 exhibit a favourable load–deformation characteristic and have collapsing strokes approaching 94% of their original diameters. An obvious trend can be seen and as the tube ellipticity ratio increases, crushed strain increases.

For *CFE* it is also evident that all the tubes displayed an acceptable stable load-carrying capacity along the crushing process. Among the tested specimens, elliptical tubes with a/b ratio of 2 displayed the highest crush force efficiency

of 0.95 and highest mean crush failure load value of 1477 N. This result also illustrated the excellent structural integrity of elliptical tubes with a/b ratio of 2. This can be supported by the appearance of load–displacement curves together with photographs of elliptical tubes with a/b ratio of 2.

Generally, the specific energy absorption of the tubes increases almost linearly with displacement and its rate is slower during the initial collapse stage. Variation of collapse initiation and collapse propagation energy absorption of the tubes with their ellipticity ratio has been plotted in Fig. 8. Similar trends were observed for collapse initiation and propagation energy absorption capabilities, in which deviation from circular cross-section results in better energy absorption capability. From the specific energy–ellipticity ratio curves of these sets shown in Fig. 8, it is observed that the specific energy absorbed by elliptical tubes (i.e. $a/b \neq 1$) increases with increase or decrease in a/b. Among the tested specimens, elliptical tubes with a/b ratio of 2 displayed the highest energy absorbed value of 700 J/kg, while tube with a/b ratio of 1.00 (i.e. circular tube) recorded the lowest value of 330 J/kg.

However, to better appreciate the variation of volumetric energy absorption capability, it can be plotted as function of ellipticity ratio. Variations in E_V of laterally crushed composite tubes are shown in Fig. 9. The volumetric energy absorption capability shows symmetry in its variation about ellipticity ratio of 1 (i.e. circular tubes). It may be noted that E_V monotonically decreases as ellipticity

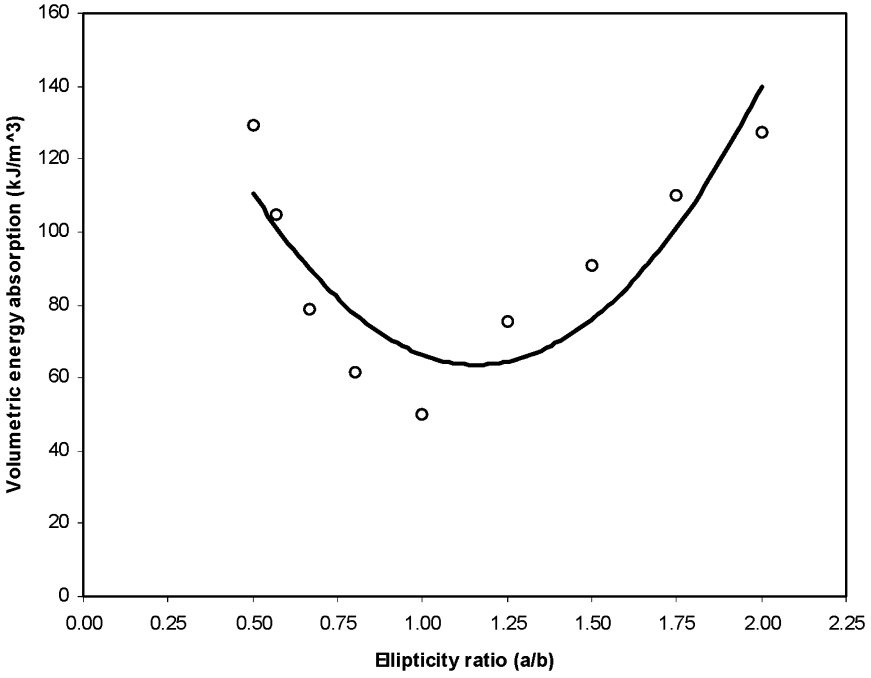

Figure 9. Volumetric energy absorption capability of laterally crushed elliptical tubes.

ratio increases until it reaches 1, after which it increases monotonically as ellipticity ratio increases. It is interesting to conclude that there is a strong tendency of only two sets: (1) $a/b < 1$ and (2) $a/b > 1$. The experimental data obtained fit the following empirical equation:

$$E_{\mathrm{V}} = 108.34(a/b)^2 - 251.37(a/b) + 209.32. \tag{4}$$

4. ENERGY DISSIPATION MECHANISMS

4.1. Micro mechanisms (W_{micro})

Microscopic investigation has been carried out to explain the failure mechanism at micro level throughout the crushing process. It is observed that the energy absorbed by the tube is dissipated to crack the matrix at the top end of the specimens. As the crush failure load is further increased, the density and extent of the matrix cracks progress such that interfacial debonding occurs and leaving the fibres unsupported, more compliant, and less likely to fail by micro buckling. Generally, the energy absorbed during this failure stage can be written as

$$W_{micro} = W_{mc} + W_{fd} + W_{bf} + W_{ld}, \tag{5}$$

where W_{mc} is the energy required to craze, crack the matrix and increase the density of matrix cracks (see Fig. 10a). It is well understood that in polymer matrix systems, cracks are often initiated at locations where several fibres debond from the matrix under load. The matrix crack growth process is probably time-dependent and one should relate the growth rate to loading history.

W_{fd} is the energy required to debond the woven roving fabric fibre from the matrix (see Fig. 10b). W_{bf} is the energy required to break and crush the fibres (see Fig. 10c). W_{ld} is the energy dissipated in local delamination (see Figs 10c and 10d).

The net effect of these energy absorption mechanisms on the total energy absorbed is difficult to quantify. However, as the developed strain is further increased, the density and extent of the matrix cracks progress such that interfacial debonding occurs and leaving the fibres unsupported, more compliant, and less likely to fail by shearing. This in turn leads to delamination, then fibre breakage and finally, degrading of the material properties at the crush zone.

It is of important to state that the contribution of micro mechanism is significantly influenced by the tube crushed strain. As the crushed strain increases, the contribution of micro mechanism increases.

4.2. Macro mechanisms

Analysis of energy dissipation mechanisms is performed in order to give some explanations for the experimental results, but also to obtain conditions for the appropriate choice of a/b for the tubes. Figure 11 shows the free body diagram of quarter of an elliptical tube in equilibrium condition. Two distinct failure modes

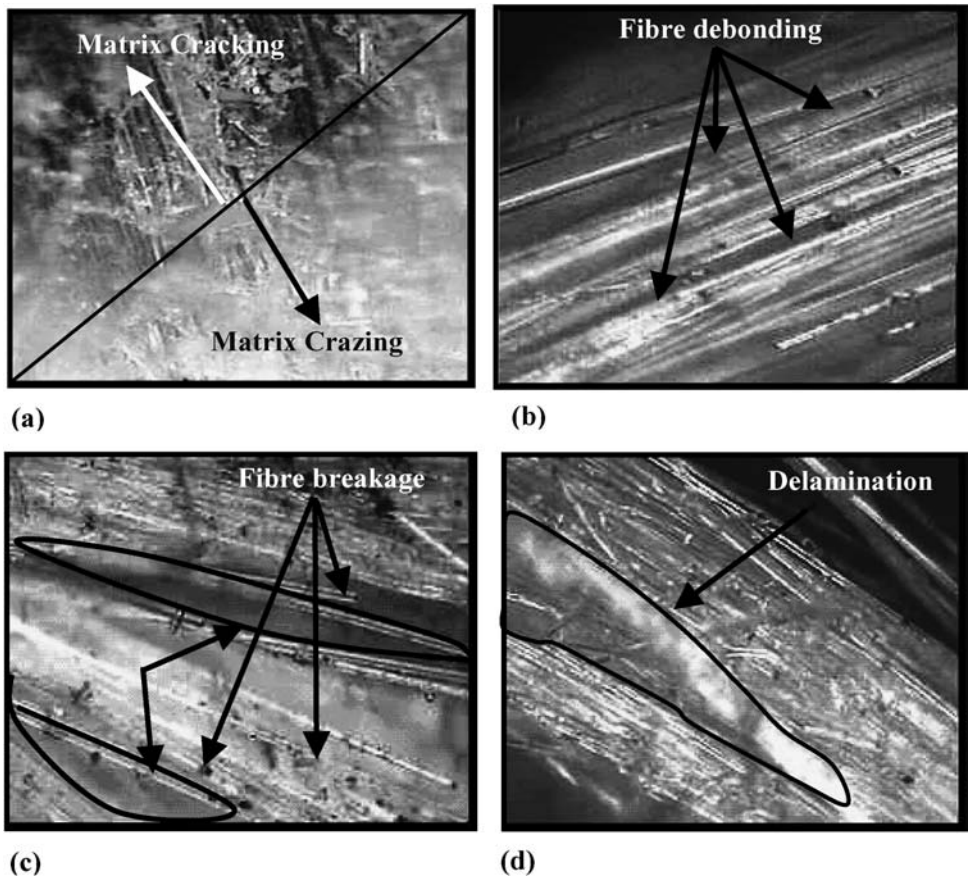

Figure 10. (a) Matrix cracking mode with magnification of 100μ; (b) Fibre debonding from the matrix mode with magnification of 100μ; (c) Fibre breakage mode with magnification of 100μ; (d) local delamination with magnification of 100μ.

were observed to dominate failure mechanisms could be identified and classified as follows.

4.2.1. Mechanism 1, Set 1. The energy dissipation during the lateral crushing of Set 1 can be written as

$$W_{Macro} = W_{fl} + W_{cd} + W_f. \tag{6}$$

Energy dissipated in flexure (W_{fl}). The energy dissipated in flexure and can be written as:

$$W_{fl} = \int \frac{M^2}{2EI}\,\mathrm{d}s, \tag{6a}$$

where ds is the curved elemental length $\mathrm{d}s = R\mathrm{d}\theta = (a_0 - \delta)\sec\theta\,\mathrm{d}\theta$; I is the moment of inertia of the tube, given by $I = \pi(b_0 a_0^3 - ba^3)/4$; E is the effective

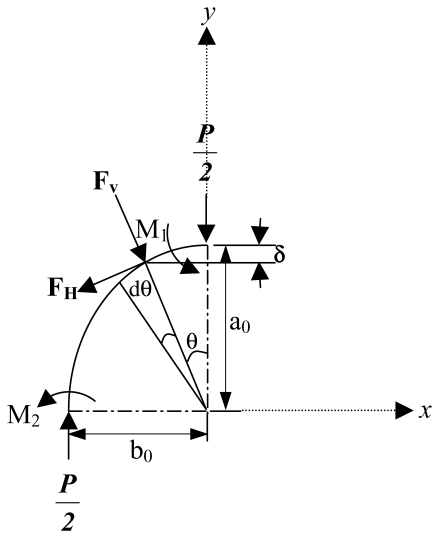

Figure 11. Free body diagram of quarter of an elliptical tube in equilibrium condition.

modulus of elasticity; M is the bending moment in tube at angle θ with semi x-axis and can be written as:

$$M = M_1 - F_H(a_0 - \delta)\sec\theta,$$

in which $F_H = \frac{P}{2}\sin\theta$, therefore,

$$M = M_1 - \frac{P}{2}(a_0 - \delta)\tan\theta,$$

here, P is the crushing load and M_1 is the moment at the top of the tube as shown in Fig. 1. If these values are substituted into equation (2a) we get

$$W_{fl} = \frac{4(a_0 - \delta)}{2\pi E(b_0 a_0^3 - ba^3)} \int_0^{\pi/2} \frac{\left(M_1 - \frac{P}{2}(a_0 - \delta)\tan\theta\right)^2}{\cos\theta}\,\mathrm{d}\theta. \qquad (6a1)$$

For tubes with circular cross-sectional area $\delta = 0$ and $a_0 = b_0$.

Energy dissipated in circumferential deformation (W_{cd}). The energy dissipated in circumferential deformation is written as

$$W_{cd} = \int \frac{F_H^2}{2AE}\,\mathrm{d}s = \int_0^{\pi/2} \frac{(P/2)^2\sin^2\theta}{2WtE}(a_0 - \delta)\sec\theta\,\mathrm{d}\theta. \qquad (6b)$$

Energy dissipated in forming fracture lines (W_f). The energy dissipated in forming fracture lines is a function of developed failure strain. It increases as the number of fracture lines increases.

All the above terms are observed to be directly or indirectly sensitive to ellipticity ratio of the tubes. The basic energy dissipation mechanisms are bending of the top and bottom of the tube and circumferential deformation of the tube side walls. When a/b is small, the developed strain does not exceed that for forming an elastic hinge at the bottom side or fracturing the tube wall. In addition within the limitation of small deformation, such tube showed plate behaviour in resisting the lateral loading. This is observed to occur for tubes with a/b ratio equal to 0.5. On the other hand, for tubes with relatively large a/b ratio, enough strains were developed to form an elastic hinge at the bottom and even to fracture the outermost surface of the tube wall.

4.2.2. Mechanism 2, Sets 2 and 3. This mechanism is associated with Sets 2 and 3 and the total work done (W_T) can be written as

$$W_{\text{Set 2\&3}} = W_{fd} + W_m + W_{fh} + W_{fl} + W_f + W_{fr}, \tag{7}$$

where W_{fd} is the energy dissipated in flattening deformation, which is observed to be non-significant. W_m is energy absorbed by columns formed at the left and right hand side of the tube wall, which is found to be very significant. W_{fh} is the energy dissipated in forming elastic hinges, which contributes significantly to the total absorbed energy. W_{fl} is the energy dissipated in flexure, which is clearly seen to be localised at the hinges and since the considered tubes are composed of the same materials but have different dimensions, the flexural energy dissipation is strongly influenced by the a/b ratio. W_f is the energy dissipated in forming fracture lines and is a function of developed failure strain. It increases as the number of fracture lines increases. W_{fr} is the energy associated with friction force. Frictional energy occurs after formation of fracture lines due to sliding of fractured outer most surface against both each other and the crushing platens.

For Set 3, the amount of fracture energy is observed to be almost the same, since all the tubes have collapsed along two longitudinal fracture lines. The difference in energy absorption capabilities comes from the effect of the column (i.e. W_m) formed at the left and right hand side of the tube wall, which increases as the a/b ratio increases. This can also be supported by the fact that structural materials are generally far more efficient in extension rather than in flexure. Also, the intertwining fibre architecture used prevents tube global buckling as well as the gross delamination at the sides of the tube wall. The woven roving fibre also prevented the tube wall from splitting the fracture along fracture lines like the unidirectional-filament fibres composite-based structures. This is because (0/90°) cross-ply reduces the interlaminar cracks propagating between layers in which the intertwining fibres support each other to carry the applied load. This load resistance mechanism in turn resulted in a large amount of energy dissipation compared with the filament fibres. This is also true for Set 2. However, the main differences between these sets are the energy dissipated in forming elastic hinges (W_{fh}) and the energy dissipated in forming fracture lines (W_f). On one hand, the number of

elastic hinges for Set 2 is less than the one for Set 3. This implies high values of W_{fh} for Set 3 over Set 2, which indicates their ability to encourage the formation of many elastic hinges.

5. EFFECT OF HINGE FORMATION

As mentioned earlier, laterally loaded tubes could result in a smooth load–deformation curve, but with low energy absorption capability. One way to improve the latter is to mitigate the failure mechanism by encouraging the formation of more hinges throughout the crushing process. Elastic bending moments at the top and side of the specimen are M_1 and M_2, respectively. The initial relationship between them can be written as $M_2 = M_1 - (P/2)b_0$. However, as the value of M_2 is less than M_1, the formation of elastic hinges and fracture lines were found to be formed and initiated at the top end of specimen in all tests. It is clear that the value of M_2 depends on the b value, which in turn is influenced by the a/b ratio. As the a/b ratio increases, the b value decreases and M_2 increases. The computed high value of M_2 for Set 3 implies high values of W_{fh}. For Set 1, the high value of b results in a low value of bending moment, which in turn results in less or even no elastic hinges formed during the crushing process. This might be the main reason behind the superiority of Set 3, where high stresses develop first at the top and bottom of the tube and lead to the formation of elastic hinges at these location, while the other two elastic hinges form later at the side of the tube. Moreover, the formation of elastic hinges makes a pronounced contribution of energy absorbed by the tubes. The elastic work done is significantly influenced by the developed strain, which is computed to be high for Set 3. In addition, the superiority of Set 3 might also be strongly attributed to their resistance mechanism to the lateral loading, which includes the combination of in-plane forces and transverse shearing forces. This combination mechanism distinguishes bending of this set from other sets.

6. SPECIMEN RECOVERY

A significant recovery of deformation is observed in the experiments. Figure 12 shows the photographs of tubes after removing the load. It is also evident that the recovery degree of tubes after being crushed is highly influence by the a/b ratio. Accordingly, as the a/b ratio increases, the recovery degree increases. This exhibits a notable flexibility of Set 3. The elastic hinges were observed to be formed at Set 3 side walls, where the severe two fracture lines were formed. Only one severe fracture line was observed at the elastic hinges of tubes with $a/b = 1.25$. It is also evident that no severe fracture lines were observed at the top and bottom part of the tube, where elastic hinges were formed. On the other hand, Set 1 did not show any formation of either hinges or fracture lines; this is due to its small curvature of the generators. This implies that increase in radius of curvature of the elliptical tubes shows a significant increase in their energy absorption capability.

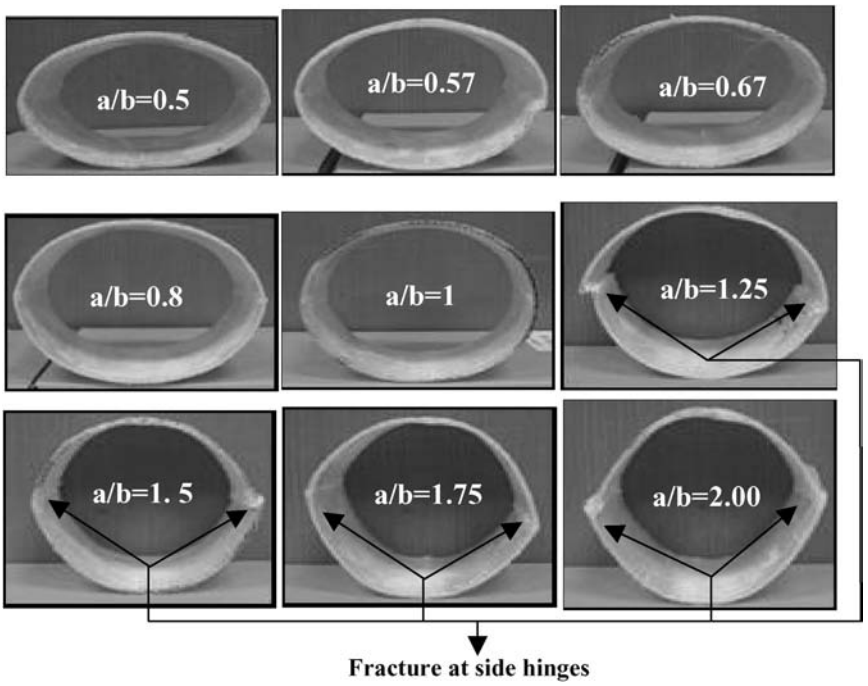

Figure 12. Recovered specimens after removing the load.

7. CONCLUSION

The behaviour of circular and elliptical tubes subjected to lateral compressive load has been examined. Two principal modes of energy dissipation mechanism have been identified. Based upon the experimental and numerical results the following conclusions can be drawn:

1. Considerable increase can be obtained for both the carrying capacity and the energy absorption capability by employing tubes with elliptical cross-section rather than the circular one.
2. Increase or decrease in ellipticity ratio improves significantly the energy absorbed by laterally compressed tubes.
3. Recovery is more if the tube ellipticity ratio is large.
4. The energy absorption capability shows symmetry in their variation about ellipticity ratio of 1 (i.e. circular tubes).
5. The number of elastic hinges was found to depend on ellipticity ratio and the number of elastic hinges increases as the ellipticity ratio increases.
6. When the tube ellipticity ratio is intermediate (i.e. Set 2) the deformation starts at the same location as Set 1 and then change as the deformation proceed to that of Set 3.

7. The contribution of membrane resistance mechanism increases as a/b ratio increases.

Acknowledgements

The authors wish to thank University Putra Malaysia for the financial support for this research programme.

REFERENCES

1. O. Alkolose, E. Mahdi and A. M. S. Hamouda, Axial crushing of elliptical composite tubes between flat platens, *Int. J. Applied Compos.* **10**, 6339–6363 (2003).
2. J. F. Carney, Modelling of steel tube vehicular crash cushion, *ASCE J. Transportation Engng* **109**, 331–346 (1983).
3. W. Johnson and S. R. Reid, Metallic energy dissipating systems, *Appl. Mech. Rev*. **31**, 277–288 (1978).
4. A. R. Watson, S. R. Reid and W. Johnson, Large deformation of thin walled circular tubes under transverse loading-I, *Int. J. Mech. Sci.* **18**, 325–333 (1976).
5. A. R. Watson, S. R. Reid, W. Johnson and S. G. Thomas, Large deformation of thin walled circular tubes under transverse loading-II, *Int. J. Mech. Sci.* **18**, 387–397 (1976).
6. A. R. Watson, S. R. Reid and W. Johnson, Large deformation of thin walled circular tubes under transverse loading-III, *Int. J. Mech. Sci.* **18**, 501–509 (1976).
7. T. Y. Reddy and S. R. Reid, Lateral compression of tubes and tube-systems with side constraints, *Int. J. Mech. Sci.* **21**, 187–199 (1979).
8. E. Mahdi, A. M. S. Hamouda and B. B. Sahari, Axial and lateral crushing of filament wound laminated composite curved compound system, *Int. J. Adv. Compos. Mater.* **11**, 171–192 (2002).
9. N. K. Gupta and H. Abbas, Lateral collapse of composite cylindrical tubes between flat platens, *Int. J. Impact Engng* **24**, 329–346 (2000).
10. L. Wu and J. F. Carney, Experimental analyses of collapse behaviours of braced elliptical tubes under lateral compression, *Int. J. Mech. Sci.* **40**, 761–777 (1998).
11. L. Wu and J. F. Carney, Initial collapse of braced elliptical tubes under lateral compression, *Int. J. Mech. Sci.* **39**, 1023–1036 (1997).
12. R. H. Burton and J. M. Craig, An investigation into the energy absorbing properties of metal tubes loaded in the transverse direction, B.Sc. Report, University of Bristol (1963).